

Fluid-crystal coexistence for proteins and inorganic nanocolloids: Dependence on ionic strength

Peter Prinsen and Theo Odijk^{a)}

Complex Fluids Theory, Faculty of Applied Sciences, Delft University of Technology, 2628 BC Delft, The Netherlands

(Received 11 April 2006; accepted 19 July 2006; published online 18 August 2006)

We investigate theoretically the fluid-crystal coexistence of solutions of globular charged nanoparticles such as proteins and inorganic colloids. The thermodynamic properties of the fluid phase are computed via the optimized Baxter model P. Prinsen and T. Odijk [J. Chem. Phys. **121**, 6525 (2004)]. This is done specifically for lysozyme and silicotungstates for which the bare adhesion parameters are evaluated via the experimental second virial coefficients. The electrostatic free energy of the crystal is approximated by supposing the cavities in the interstitial phase between the particles are spherical in form. In the salt-free case a Poisson-Boltzmann equation is solved to calculate the effective charge on a particle and a Donnan approximation is used to derive the chemical potential and osmotic pressure in the presence of salt. The coexistence data of lysozyme and silicotungstates are analyzed within this scheme, especially with regard to the ionic-strength dependence of the chemical potentials. The latter agree within the two phases provided some upward adjustment of the effective charge is allowed for. © 2006 American Institute of Physics. [DOI: 10.1063/1.2336423]

I. INTRODUCTION

One current view of protein crystallization centers on the second virial coefficient B_2 being a relevant quantity determining the onset of crystallization.¹⁻⁴ There exists a crystallization slot of negative B_2 values which expresses a necessary range of solution conditions for adequate crystals to grow. A negative value of B_2 implies a Baxter stickiness parameter as it is conventionally defined via B_2 only and we here denote by τ_0 . Thus, in a similar vein, there have been attempts to correlate τ_0 with the solubility of nanoparticles in explaining fluid-crystal coexistence curves.^{5,6}

The free energy of a suspension of particles cannot, of course, depend on B_2 alone. In a recent paper⁷ we introduced a new analytical theory for protein solutions in which the real fluid is replaced by a suspension of spheres with an appropriately chosen adhesion of the Baxter type. The stickiness parameter τ is computed by a variational principle for the free energy instead of via B_2 . In our optimized Baxter model, τ is not at all identical to τ_0 ; τ depends not only on the ionic strength but also on the protein concentration. In Ref. 5, Rosenbaum *et al.* plotted τ_0 logarithmically as a function of the nanoparticle concentration which effectively coarse-grains the experimental data they show. If we zoom in on their curve, there is a lot of fine detail which we here argue to be related to the fact, in part, that τ is a better similarity parameter. In particular, we seek to understand the ionic-strength dependence of the fluid-crystal coexistence curves by going beyond theory based solely on τ_0 .

We have recently tested the optimized Baxter model on a

system of spheres interacting via an attractive Yukawa potential analyzed by computer simulations.⁸ The stickiness parameter τ , evaluated by optimizing the free energy, is indeed a useful similarity variable for gaining insight into the pressures and chemical potentials from simulations of the fluid phase. The magnitudes of these quantities are also well predicted by the optimized Baxter model. However, τ is not a correct similarity variable to describe fluid-crystal coexistence as we show in Appendix A, in view of the fact that the weighting of configurations is different in the respective phases.

Here, we will not focus on the variable τ and the fluid phase but rather on the coexistence itself. The systems we study are assumed to have a short enough range so that the coexistence between two fluid phases is apparently circumvented. An *a priori* theory is problematic because we would need a quantitative theory of the crystal phase in terms of postulated attractive forces which are currently unknown. Theoretical efforts exist in the literature⁹⁻¹¹ at the expense of introducing unknown parameters which we want to avoid here. We do not present conventional phase diagrams because we do not know the right thermodynamic variable to plot to get a universal diagram of states. The variable τ itself is not useful as we show in Appendix A.

In practice, it may be very difficult to achieve ideal thermodynamic equilibrium between the liquid phase and some crystalline state. Equilibrium may not have been reached, the crystal could be heterogeneous and the formation of aggregates could complicate the attainment of equilibrium (see, for instance, the discussion by Cacioppo and Pusey on lysozyme¹²). Nevertheless, it may still be useful to assume that equilibrium is ideally attained provided our goal is sufficiently modest. The balance of chemical potentials has been

^{a)} Author to whom correspondence should be addressed. Present address: P.O. Box 11036, 2301 EA Leiden, The Netherlands. Electronic mail: odijkctf@wanadoo.nl

used before to acquire information about the crystal from the solubility in the fluid phase.³ Our concern here will be to try to gain insight into the ionic-strength dependence of the thermodynamic properties of the crystal. We may argue that this dependence could be approximated by a Donnan equilibrium so it would not be very sensitive to the precise crystal habit adopted. We therefore compute the protein chemical potential and osmotic pressure of the coexisting liquid phase at the experimentally determined solubility with the help of the optimized Baxter model. We then investigate whether their dependence on the electrolyte concentration agrees with that predicted by a simple crystal model. The theory is applied to a protein (lysozyme) and an inorganic nanocolloid [silicotungstate (STA)].

II. OPTIMIZED BAXTER MODEL

We first discuss how we obtain the bare adhesion parameters via the second virial coefficient, and then summarize the optimized Baxter model,⁷ which is an appropriate liquid state theory provided we use the right stickiness parameter τ as emphasized in the Introduction. We consider a system of charged nanometer-sized particles (e.g., proteins or nanocolloids) in water with added monovalent salt of ionic strength I . We suppose the particles are spherical with radius a . The charge is distributed uniformly on the particle's surface. For convenience, all distances in this section will be scaled by the radius a and all energies by $k_B T$, where k_B is Boltzmann's constant and T is the temperature. Because monovalent ions (counterions and salt ions) are present in solution, the Coulomb repulsion between the particles will be screened and it is here given by a far-field Debye-Hückel potential.⁷ The effective number Z_{eff} of charges on the sphere (taken to be positive) will here be computed in the Poisson-Boltzmann approximation. We let the attraction between two particles be of range much shorter than their radius, and we model it by a potential well of depth U_A and width $\delta \ll 1$. Actually, the attractive interactions are, of course, much more complicated than this simple form. Dispersion forces, in particular, have been reinvestigated for small particles recently^{13,14} although the continuum approximation certainly becomes rather poor at the nanolevel dealt with here. Also, arbitrary cutoffs need to be introduced;⁷ it turns out that a simple well is quite adequate to describe the experimental data on B_2 (see Sec. III below). The total interaction $U(x)$ between two particles whose centers of mass are separated by an actual distance r is thus of the form

$$U(x) = \begin{cases} \infty, & 0 \leq x \leq 2 \\ U_{\text{DH}}(x) - U_A, & 2 \leq x < 2 + \delta \\ U_{\text{DH}}(x), & x \geq 2 + \delta, \end{cases} \quad (1)$$

$$x \equiv \frac{r}{a},$$

with Debye-Hückel interaction

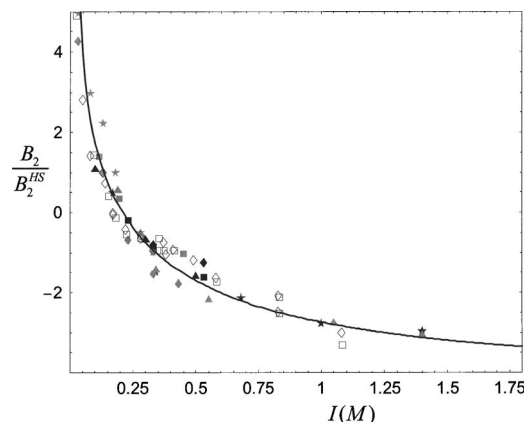


FIG. 1. The second virial coefficient of lysozyme as a function of the ionic strength. The second virial coefficient is scaled by the hard sphere value B_2^{HS} . The data are taken from a variety of experiments; see Ref. 7 for more details. The added salt is NaCl. The solid line is a fit to the data with $U_A = 2.90$ and $\delta = 0.183$.

$$U_{\text{DH}}(x) = 2\xi \frac{-e^{-\omega(x-2)}}{x}. \quad (2)$$

Here, $\xi \equiv (Q/2a)(Z_{\text{eff}}/(1+\omega))^2$ and $\omega \equiv \kappa a$, which are given in terms of the Debye length κ^{-1} defined by $\kappa^2 = 8\pi QI$ and the Bjerrum length $Q = q^2/\epsilon k_B T$, which equals 0.71 nm in water at 298 K (ϵ is the permittivity of water and q is the elementary charge); $\omega = 3.28a\sqrt{I}$, if the radius a is given in nanometers and the ionic strength I in M. We suppose 1-1 electrolyte has been added in excess so I is the concentration of added salt. We have derived the effective charge qZ_{eff} in the Poisson-Boltzmann approximation⁷

$$Z_{\text{eff}} = Z - \frac{\omega^2}{6} \left(\frac{Q}{a}\right)^2 \left(\frac{Z}{1+\omega}\right)^3 e^{3\omega} E_1(3\omega). \quad (3)$$

Here $E_1(x)$ is the exponential integral defined by $E_1(x) = \int_x^\infty dt t^{-1} e^{-t}$ and qZ is the actual charge per particle. Equation (3) is numerically consistent with a different form recently proposed by Aubouy *et al.*¹⁵ which is also valid at large values of Z .

We suppose that the bare charge on the particles as a function of the ionic strength is known from experiment, so the only unknown parameters are U_A and δ which are chosen to be independent of I . The latter are determined by fitting preferably complete experimental data of the second virial coefficient B_2 as a function of the ionic strength I at constant pH to B_2 computed numerically with the help of the expression

$$B_2 = 2\pi a^3 \int_0^\infty x^2 dx (1 - e^{-U(x)}) \quad (4)$$

using Eq. (1). We have previously done this for a wide variety of B_2 data on lysozyme at two values of the pH (4.5 and 7.5) and we were able to obtain very good fits⁷ (see, e.g., Fig. 1 which is discussed in Sec. III B).

It is important to stress that though there are two adjustable parameters δ and U_A , the actual fit in practice depends

almost solely on adjusting the single combination $\delta \exp U_A$. This is because a convenient analytical approximation of the second virial turns out to have the form⁷

$$\frac{B_2}{B_2^{\text{HS}}} \approx 1 + \frac{3\xi}{2\omega} - \frac{3}{2} e^{-\xi} \delta e^{U_A}, \quad (5)$$

and is able to describe the experimental data on lysozyme quite well with an appropriate value of $\delta \exp U_A$. Here, B_2^{HS} is the second virial coefficient pertaining to hard spheres. The strong correlation of adjustable parameters is not unusual for it is well known in the theory of gases when one attempts to fit the temperature dependence of the second virial coefficient in terms of a Lennard-Jones interaction, for instance.¹⁶ We note that Eq. (5) disagrees starkly with an approximation put forward earlier,¹⁷ both with regard to the pure electrostatic and the adhesive contributions. In particular, the third, i.e., adhesion term in Eq. (5) is not at all independent of the ionic strength but rather diminishes fast as the electrolyte concentration is lowered. Furthermore, the pure electrostatic term cannot be derived from a Donnan equilibrium as we point out in Sec. IV.

At high salt concentrations, the parameter ξ becomes small owing to screening so B_2 becomes lower than the hard sphere value, as can be seen from Eq. (5). Nevertheless, the electrostatic repulsion still exerts itself, so an effective adhesion parameter we may wish to introduce would be smaller than the bare value. We therefore adopt a similar strategy to the liquid state at finite concentrations by first introducing a suitable reference state amenable to analytical computation.⁷ This is a solution of hard spheres whose radius is still a but with a Baxter adhesion potential whose strength is defined by a suitable stickiness parameter τ . The statistical properties of this suspension as a function of the volume fraction of spheres η ($=4\pi a^3/3$ times number density) may be solved in the Percus-Yevick approximation.¹⁸ The parameter τ is adjustable and is computed via a variational principle for the free energy. The latter may be written as a functional expansion in terms of the so-called blip function which is the difference in Mayer functions of the respective interactions [Eq. (1) and the Baxter interaction].^{7,19} We set the first-order deviation from the free energy pertaining to the reference state equal to zero. This determines τ which depends not only on the well parameters δ and U_A and electrostatic variables ω and ξ but also on the volume fraction of nanospheres. It is given by⁷

$$\frac{1}{\tau} = 3\epsilon \left[(e^{U_A} e^{-[\xi/(1+\delta/2)]e^{-\omega\epsilon}} - 1)(1 + (1+H)\epsilon) + (e^{U_A} e^{-\xi} - 1) \right], \quad (6)$$

where

$$\epsilon = \delta - K^{-1}[(1 + \delta H)P_1 + HP_2], \quad (7)$$

$$P_1 = \frac{8}{\omega^2}(1 + \omega\delta)M + \frac{16}{\omega} \left(\frac{M}{1+M} \right), \quad (8)$$

$$P_2 = \frac{8}{\omega^3}(2 + \omega\delta)M + \frac{16}{\omega^2} \ln(1+M), \quad (9)$$

$$M \equiv \xi e^{-\omega\delta}/4, \quad (10)$$

$$K = 2(e^{U_A} e^{-[\xi/(1+\delta/2)]e^{-\omega\delta}} - 1)(1 + (1+H)\delta) + 2(e^{U_A} e^{-[\xi/(1+\delta/2)]e^{-\omega\epsilon}} - 1)(1 + (1+H)\epsilon), \quad (11)$$

$$H = \frac{\eta}{2\tau(1-\eta)} \left(\frac{\eta(1-\eta)}{12} \lambda^2 - \frac{1+11\eta}{12} \lambda + \frac{1+5\eta}{1-\eta} - \frac{9(1+\eta)}{2(1-\eta)^2} \frac{1}{\lambda} \right) \quad (12)$$

and λ is given by

$$\tau = \frac{1 + \eta/2}{(1-\eta)^2} \frac{1}{\lambda} - \frac{\eta}{1-\eta} + \frac{\eta}{12} \lambda. \quad (13)$$

Note that τ is readily obtained by iteration. One starts with initial values for τ and ϵ and then calculates λ , H , and K_1 from Eqs. (11)–(13). Then, a new value of ϵ at fixed H is computed iteratively with the help of Eqs. (7) and (11). Next, a new value of τ is given by Eq. (6) and then the cycle is repeated until the variables become stationary.

Having obtained the effective adhesion parameter τ , we simply calculate thermodynamic properties of the reference state within the Percus-Yevick approximation. The free energy of the actual system does deviate slightly from that of the reference state but we have shown that the deviations are very small.⁷ To compute the osmotic pressure Π we use the result from the compressibility route¹⁸ which appears to be more in line with simulations,²⁰

$$\frac{\Pi v_0}{k_B T} = \frac{\eta(1 + \eta + \eta^2)}{(1-\eta)^3} - \frac{\eta^2(1 + \eta/2)}{(1-\eta)^2} \lambda + \frac{\eta^3}{36} \lambda^3. \quad (14)$$

When the roots of Eq. (13) are complex, the pressure cannot be determined for the physical realization of the liquid state breaks down, at least with the Percus-Yevick approximation. The chemical potential μ of the spherical particles is determined by using the pressure from Eq. (14) and the Gibbs-Duhem equation at constant temperature,²¹

$$\frac{\mu - \mu_0}{k_B T} = \ln \frac{\eta}{1-\eta} + \frac{3\eta(4-\eta)}{2(1-\eta)^2} + \frac{\Pi v_0}{k_B T} + J. \quad (15)$$

Here,

$$J = \frac{3}{2} \eta^2 \lambda^2 - \frac{3\eta(1+4\eta)}{(1-\eta)} \lambda + \frac{6\eta(2+\eta)}{(1-\eta)^2} - \frac{18\eta}{1-\eta} \tau - \frac{6(\tau - \tau_c)^2}{\tau_c(1-6\tau_c)} \ln \left| \frac{\lambda(1-\eta) - \tau_c^{-1}}{\tau^{-1} - \tau_c^{-1}} \right| + \frac{6\tau_c(18\tau\tau_c - 1)^2}{1-6\tau_c} \ln \left| \frac{\lambda(1-\eta) - 18\tau_c}{\tau^{-1} - 18\tau_c} \right| \quad (16)$$

is the contribution to the chemical potential that vanishes in the hard-sphere limit ($\tau \rightarrow \infty$) and

$$\frac{\mu_0}{k_B T} = \ln \frac{1}{v_0} \left(\frac{h^2}{2\pi m k_B T} \right)^{3/2}, \quad (17)$$

where h is Planck's constant and m is the mass of a sphere. The critical value of τ , below which there is a range of den-

TABLE I. The charge Z of hen-egg-white lysozyme (from Ref. 25), the effective charge Z_{eff} (from Eq. (3)), the lowered effective charge $\bar{Z}=Z_{\text{eff}}-1$, the dimensionless interaction parameters ω , ξ , and τ , the solubility of lysozyme S , the volume fraction η , the dimensionless chemical potential $(\mu-\mu_0)/k_B T$, and the dimensionless pressure $\Pi V_0/k_B T$ as a function of the ionic strength I in the fluid phase. ξ has been calculated using the lowered effective charge \bar{Z} .

pH	I (% w/v)	I (M)	ω	Z	Z_{eff}	\bar{Z}	ξ	τ	S (g/l)	η	$\frac{\mu-\mu_0}{k_B T}$	$\frac{\Pi V_0}{k_B T}$
4.0	2.0	0.40	3.33	11.1	10.54	9.54	1.078	0.127	48.7	0.0354	-3.60	0.0308
4.0	3.0	0.57	3.97	11.2	10.74	9.74	0.851	0.096	14.0	0.0102	-4.72	0.0095
4.0	4.0	0.74	4.53	11.4	10.99	9.99	0.725	0.083	4.30	0.00313	-5.82	0.0030
4.0	5.0	0.92	5.02	11.6	11.23	10.23	0.641	0.077	3.11	0.00226	-6.13	0.0022
4.0	7.0	1.26	5.89	11.7	11.40	10.40	0.506	0.068	1.36	0.00099	-6.94	0.0010
4.5	2.0	0.40	3.33	10.2	9.76	8.76	0.909	0.107	30.1	0.0219	-4.05	0.0194
4.5	3.0	0.57	3.97	10.3	9.94	8.94	0.717	0.086	10.3	0.00750	-5.01	0.0071
4.5	4.0	0.74	4.53	10.3	10.00	9.00	0.588	0.075	5.22	0.00380	-5.64	0.0037
4.5	5.0	0.92	5.02	10.4	10.13	9.13	0.510	0.070	3.43	0.00250	-6.04	0.0024
4.5	7.0	1.26	5.89	10.4	10.19	9.19	0.395	0.063	1.87	0.00136	-6.63	0.0013
5.0	2.0	0.40	3.33	9.1	8.79	7.79	0.719	0.090	17.6	0.0128	-4.54	0.0117
5.0	3.0	0.57	3.97	9.1	8.85	7.85	0.553	0.075	7.38	0.00537	-5.33	0.0051
5.0	4.0	0.74	4.53	9.2	8.99	7.99	0.464	0.069	4.72	0.00344	-5.75	0.0033
5.0	5.0	0.92	5.02	9.2	9.02	8.02	0.394	0.064	3.63	0.00264	-6.00	0.0026
5.0	7.0	1.26	5.89	9.1	8.96	7.96	0.297	0.059	2.46	0.00179	-6.37	0.0018

sities where there is no real solution of λ , is given by

$$\tau_c = \frac{2 - \sqrt{2}}{6}. \quad (18)$$

III. SOLUBILITY CURVES: CHEMICAL POTENTIAL OF THE FLUID PHASES

A. Method

Since we suppose the crystal is in thermodynamic equilibrium with the fluid, the protein chemical potentials as well as the osmotic pressures in both phases are uniform. The chemical potentials of the counter- and coions must also be uniform but we will address this issue later within a Donnan equilibrium. Solubility data from experiment represent the particle concentration in the fluid phase as a function of the pH and the salt concentration. Thus we compute the chemical potential and the osmotic pressure of the solution with the help of the optimized Baxter model of the previous section. We have done this in two cases of nanoparticles where we have sufficient experimental data on the second virial coefficient to evaluate the well parameters U_A and δ with sufficient accuracy.

B. Lysozyme

The protein hen-egg-white lysozyme has been well characterized in aqueous solutions of simple electrolytes. We here choose the effective radius a such that the volume of the model sphere is equal to the volume of a lysozyme molecule in the tetragonal crystal state. The latter is determined from the water content of the tetragonal crystal (0.335 mass fraction²²), the crystal volume per protein molecule (29.6 nm³, based on the dimensions $7.91 \times 7.91 \times 3.79$ nm³ of the unit cell containing eight protein molecules²³), the density of the crystal [1.242×10^3 kg m⁻³ (Ref. 22)], and the density of water (0.998×10^3 kg m⁻³). Thus we have a

= 1.6 nm and note that this is 0.1 nm less than the value of 1.7 nm we used previously,⁷ which was based on approximation of the protein by an ellipsoid of dimensions $4.5 \times 3.0 \times 3.0$ nm.²⁴ For the sake of consistency we here use the single value $a=1.6$ nm in computations pertaining to both phases.

The experimental data for the second virial coefficient of lysozyme have been discussed by us at length previously⁷ and are presented in Fig. 1. For details on determining the parameters U_A and δ of the attractive potential we also refer to Ref. 7. Since we are using a smaller effective radius here, we deduce the values $U_A=2.90$ and $\delta=0.183$ which are somewhat different from those derived earlier.⁷ The values of the bare charge qZ of a lysozyme molecule as a function of the ionic strength are the same as those used in Ref. 7, i.e., they are determined by interpolation from hydrogen-ion titration data in KCl.²⁵ We assume that KCl and NaCl (see below) behave identically in an electrostatic sense. The effective charge does differ slightly because it is a function of a [see Eq. (3)]. We again use the lowered effective charge $\bar{Z}=Z_{\text{eff}}-1$ instead of the effective charge Z_{eff} in order to fit B_2 accurately at lower ionic strengths when it is dominated by electrostatics. We set U_A and δ to be independent of the pH.

Accurate data on the solubility S as a function of the NaCl concentration have been obtained by Cacioppo and Pusey¹² using column beds of tetragonal microcrystallites of lysozyme in a range of pH and temperatures. We here employ their data at 298 K and at three representative values of the pH (see Table I) The ionic strength I in M is determined from the ionic strength in % w/v by the relation $I(M) = 0.06 + 0.171 I(\% \text{ w/v})$. Here, the value 0.06 accounts for the effective ionic strength of the 0.1M sodium acetate buffer used and $0.171 = 10/M_{\text{NaCl}}$ where $M_{\text{NaCl}} = 58.44$ g mol⁻¹ is the molar mass of NaCl. The dimensionless parameter ω is then given by $\omega = 5.25\sqrt{I}$, where I is given in M_i and $\xi = 0.222(\bar{Z}/(1+\omega))^2$.

The volume fraction η of protein in the liquid phase is

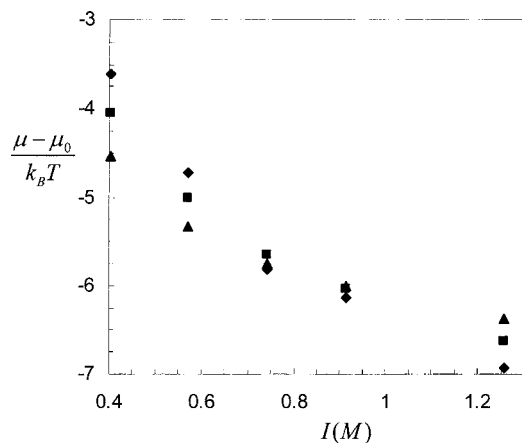


FIG. 2. The dimensionless chemical potential of lysozyme in the fluid phase as a function of the ionic strength at pH 4.0 (diamonds), pH 4.5 (squares), and pH 5.4 (triangles). See also Table I.

given by $\eta = SN_A v_0 / M$, where N_A is Avogadro's number, $v_0 = 4\pi a^3 / 3$ is the volume of a lysozyme molecule, and $M = 14.3 \times 10^3 \text{ g mol}^{-1}$ (Ref. 26) is the molar mass of lysozyme. The parameter τ describing the effective adhesion is determined as described in Sec. II [see Eqs. (6)–(13)], using the values $U_A = 2.90$ and $\delta = 0.183$. Then, the dimensionless chemical potential $(\mu - \mu_0) / k_B T$ and the dimensionless osmotic pressure $\Pi v_0 / k_B T$ are determined from Eqs. (15) and (14), respectively (see Table I). Figure 2 shows the chemical potential as a function of the ionic strength I at three different values of the pH. Figure 3 shows the osmotic pressure under the same conditions.

C. Silicotungstates (STA)

The next system we consider is STA in water with three different kinds of added salt: NaCl, HCl, and LiCl. STA molecules are spherical, more or less (see Fig. 2 in Ref. 27), with an effective diameter of 1.1 nm,^{28,29} so we set $a = 0.55 \text{ nm}$. The structural formula for the polyanion $\text{SiW}_{12}\text{O}_{40}^{4-}$ implies a molar mass $M_{\text{STA}} = 2874.3 \text{ g mol}^{-1}$. We assume that the pH is low enough for the molecule to be fully dissociated, i.e., $Z = 4$.

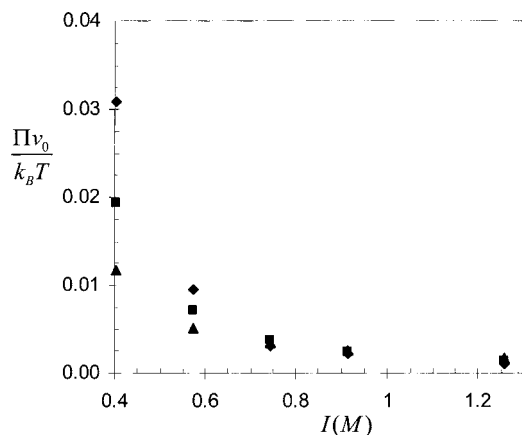


FIG. 3. The dimensionless pressure of lysozyme in the fluid phase as a function of the ionic strength at pH 4.0 (diamonds), pH 4.5 (squares), and pH 5.4 (triangles). See also Table I.

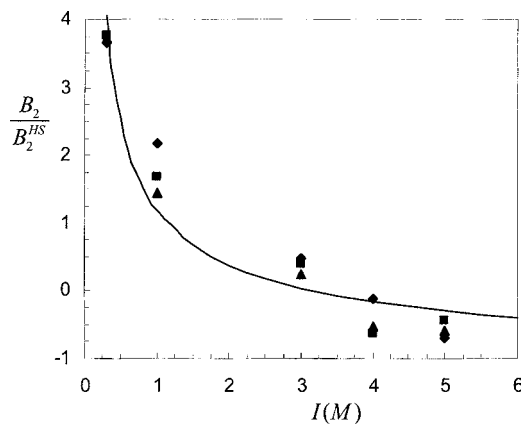


FIG. 4. The second virial coefficient of STA as a function of the ionic strength. The second virial coefficient is scaled by the hard sphere value B_2^{HS} . The experimental data are taken from Zukoski *et al.* (Ref. 30). The added salt is LiCl (diamonds), HCl (squares), and NaCl (triangles), respectively, and in all cases the counterion of STA is the same as that of the salt. The solid line is a fit to the experimental data with $U_A = 3.30$ and $\delta = 0.05$.

We determine the well parameters U_A and δ for the attractive interaction by fitting experimental data of the second virial coefficient in the same way as was done for lysozyme,⁷ except we now do not adjust Z_{eff} . The second virial coefficients for Li_4STA , H_4STA , and Na_4STA are taken from Ref. 30 and plotted in Fig. 4. In each case, the added salt is $X\text{Cl}$, where X represents the counterion of the crystal. The values of the dimensionless parameters $\omega = 1.80\sqrt{I}$, $\xi = 0.645(Z_{\text{eff}} / (1 + \omega))^2$, Z , and Z_{eff} pertaining to the data in Fig. 4 are given in Table II. We have set $\delta = 0.05$. A least squares fit to the data represented in Fig. 4 then gives $U_A = 3.30$. In fact, there is a range of combinations of δ and U_A that yield almost the identical curve as long as $\delta \exp U_A \approx 1.36$ and $\delta \ll 1$, so our choice of $\delta = 0.05$ is a bit arbitrary. This similarity with respect to the sole parameter $\delta \exp U_A$ is in accord with our approximation for B_2 given by Eq. (5).

The solubilities for Li_4STA , H_4STA , and Na_4STA have been measured by Zukoski *et al.*,³⁰ where the same electrolytes are used as in the measurements of B_2 (see Table III). The volume fraction η of STA is given by $\eta = SN_A v_0 / M_{X_4\text{STA}}$, where S is the solubility of STA (note that here it is given in g/ml, whereas for lysozyme it was given in g/l), $v_0 = 4\pi a^3 / 3$ is the volume of a STA molecule and $M_{X_4\text{STA}}$ is the molar mass, where X again represents the counterion in the respective cases. We have $M_{\text{H}_4\text{STA}} = 2878.3 \text{ g mol}^{-1}$, $M_{\text{Li}_4\text{STA}} = 2902.0 \text{ g mol}^{-1}$, and $M_{\text{Na}_4\text{STA}} = 2966.2 \text{ g mol}^{-1}$. The stickiness parameter τ is determined

TABLE II. Values of the bare charge Z of STA, the effective charge Z_{eff} [from Eq. (3)] and the dimensionless interaction parameters $\omega = 1.80\sqrt{I}$ and $\xi = 0.645(Z_{\text{eff}} / (1 + \omega))^2$ as a function of the ionic strength I . These entries apply to the data plotted in Fig. 4.

$I(M)$	ω	Z	Z_{eff}	ξ
0.3	0.99	4.0	3.42	1.905
1.0	1.80	4.0	3.58	1.054
3.0	3.13	4.0	3.76	0.536
4.0	3.61	4.0	3.80	0.439
5.0	4.03	4.0	3.83	0.373

TABLE III. The charge Z of STA, the effective charge Z_{eff} [from Eq. (3)], the dimensionless interaction parameter ω , ξ and τ , the solubility S of $X_4\text{STA}$, the volume fraction η , the dimensionless chemical potential $(\mu - \mu_0)/k_B T$, and the dimensionless pressure $\Pi V_0/k_B T$ as a function of the ionic strength I in the fluid phase. Here the counterion is X^+ and the added salt is $X\text{Cl}$. ξ has been calculated using the effective charge Z_{eff} .

X	$I(M)$	ω	Z	Z_{eff}	ξ	τ	S (g/ml)	η	$\frac{\mu - \mu_0}{k_B T}$	$\frac{\Pi V_0}{k_B T}$
H	1.0	1.80	4.0	3.58	1.054	0.786	1.94	0.284	1.30	0.706
H	2.0	2.55	4.0	3.70	0.700	0.358	1.67	0.243	-0.48	0.375
H	3.0	3.13	4.0	3.76	0.536	0.255	1.36	0.198	-1.40	0.226
H	4.0	3.61	4.0	3.80	0.439	0.215	1.11	0.162	-1.91	0.158
H	5.0	4.03	4.0	3.83	0.373	0.193	0.57	0.0830	-2.65	0.077
Li	1.0	1.80	4.0	3.58	1.054	0.668	2.15	0.312	1.55	0.811
Li	2.0	2.55	4.0	3.70	0.700	0.352	1.85	0.267	-0.267	0.433
Li	3.0	3.13	4.0	3.76	0.536	0.255	1.36	0.197	-1.41	0.224
Li	4.0	3.61	4.0	3.80	0.439	0.215	0.81	0.118	-2.23	0.114
Li	5.0	4.03	4.0	3.83	0.373	0.193	0.32	0.0469	-3.16	0.045
Na	1.0	1.80	4.0	3.58	1.054	0.906	1.85	0.262	1.07	0.625
Na	2.0	2.55	4.0	3.70	0.700	0.359	1.67	0.236	-0.54	0.358
Na	3.0	3.13	4.0	3.76	0.536	0.255	1.36	0.192	-1.44	0.218
Na	4.0	3.61	4.0	3.80	0.439	0.215	0.74	0.104	-2.35	0.100
Na	5.0	4.03	4.0	3.83	0.373	0.193	0.46	0.0657	-2.86	0.062

by the method described in Sec. II [see Eqs. (6)–(13)], using the values $U_A = 3.30$ and $\delta = 0.05$. The chemical potential and the osmotic pressure are again determined from Eqs. (15) and (14), respectively (see Table III). We display these thermodynamic variables as a function of the ionic strength in Figs. 5 and 6.

IV. CRYSTAL MODEL: DONNAN EFFECT

Having computed the thermodynamic properties of the fluid phases of lysozyme and STA, and hence those of the respective crystal phases under the assumption of equilibrium of the two phases, we now attempt to gain insight into them by introducing a simple model for the crystal. In the latter the spherical particles either touch or are very close. There are thus minute “surfaces of interaction” where the forces between two nearby spheres are predominantly attractive. It is therefore reasonable to write the thermodynamic

potential Ω of a crystal of N spheres in a volume V as a superposition of attractive and electrostatic contributions to a first approximation,

$$\Omega = \frac{1}{2}k(c)\frac{(V - V_0)^2}{V_0} + Nf_{\text{el}}(c, I_c) + \Pi(S, I)V - \mu(S, I)N. \quad (19)$$

The crystal is immersed in a large reservoir at a constant osmotic pressure Π and chemical potential μ containing a saturated solution of nanospheres at a solubility S and ionic strength I [Π and μ are given by Eqs. (14) and (15), respectively]. The crystal has elastic properties denoted by the modulus k which depends on the density $c = N/V$ and the crystal would have a volume V_0 in the absence of electrostatic forces ($|V - V_0| \ll V_0$). Actually, the form of the elastic energy is more complicated and depends on the precise crystal habit³¹ but the simple harmonic form in Eq. (19) suffices for our purposes. There is a Donnan equilibrium (see below)

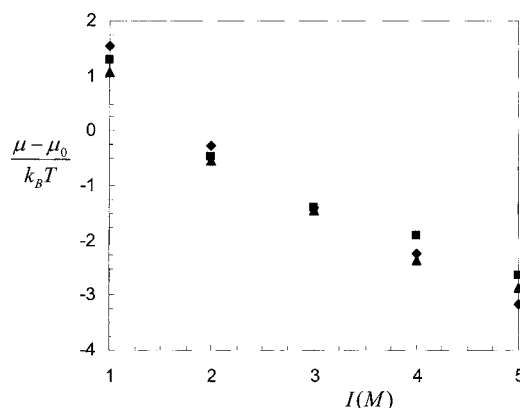


FIG. 5. The dimensionless chemical potential of STA in the fluid phase as a function of the ionic strength. The added salt is LiCl (diamonds), HCl (squares), and NaCl (triangles), respectively, and in all cases the counterion of STA is the same as that of the salt. See also Table III.

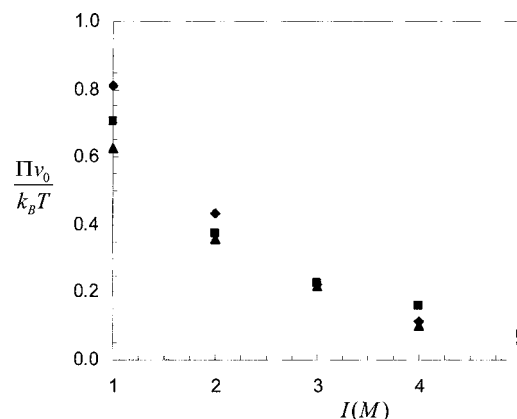


FIG. 6. The dimensionless pressure of STA in the fluid phase as a function of the ionic strength. The added salt is LiCl (diamonds), HCl (squares), and NaCl (triangles), respectively, and in all cases the counterion of STA is the same as that of the salt. See also Table III.

which leads to a salt concentration I_c within the interstitial region in the crystal. We adopt a continuum approximation: the electrostatic free energy Nf_{el} is computed for a lattice of charged spheres embedded in a solvent of uniform permittivity ϵ and electrolyte concentration I_c .

At equilibrium, Ω must be minimized ($\partial\Omega/\partial V=0$; $\partial\Omega/\partial N=0$) so that

$$\Pi \approx \Pi_{el} - k \left(\frac{V - V_0}{V_0} \right) + \frac{1}{2} c \frac{dk}{dc} \left(\frac{V - V_0}{V_0} \right)^2, \quad (20)$$

$$\mu \approx \mu_{el} + \frac{1}{2} \frac{dk}{dc} \left(\frac{V - V_0}{V_0} \right)^2. \quad (21)$$

We have introduced the electrostatic counterparts of the osmotic pressure and the chemical potential of a charged sphere in the crystal phase on the right hand sides of Eqs. (20) and (21). In Eq. (20) the elastic term proportional to k may easily be of order Π_{el} but the quadratic form is negligible. In view of the fact that $\Pi_{el} = O(c\mu_{el})$, we then have $\mu \approx \mu_{el}$ to a good approximation from Eq. (21). In effect, as we change the ionic strength of the fluid phase, the solubility S and the salt concentration I_c within the crystal readjust themselves whereas the volume V remains virtually constant. The chemical potential is modified only by virtue of the change in electrostatic shielding about a sphere in the lattice. But a substantial hydrostatic pressure may be exerted within the crystal as we decrease its volume a bit.

Next, we compute the electrostatic properties of the crystal. The colligative properties of salt-free polyelectrolytes are often addressed in terms of a cell model in which a test cylinder is surrounded by a boundary of similar symmetry on which the electric field vanishes.³² The boundary effectively replaces the effect of the surrounding particles on the test particle. This picture is reasonable at low volume fractions but must break down at high concentrations when the electric field is highly heterogeneous. In the latter case, one of us has advocated focusing on the voidlike regions instead of on a test particle (see Ref. 33 which deals with a hexagonal lattice of DNA at very high concentrations). Thus, in a crystal of spheres we may distinguish very small regions between particles that almost touch which we view as thin boundary layers, and larger voids which we will simply approximate by spheres. (We are here concerned with spheres of high charge density which leads to counterions being “condensed.” At low charge densities, it is possible to give a more general analysis; see Appendix B). Discrete charge effects should prevail when evaluating the electrostatics of the boundary layers. These energies are here assumed to be independent of the ionic strength since the relevant scales in the boundary layers are very small in crystals of nanoparticles.

We therefore first solve the Poisson-Boltzmann equation for a charged void or spherical cavity of radius b without salt and then discuss the effect of monovalent salt via a Donnan equilibrium. The charge density on the surface of the cavity is uniform and the total number of charges is Z . In view of electroneutrality there are Z counterions in the cavity, each bearing charge $-q$. Within a mean-field analysis, the counter-

ion density $\rho(r)$ inside the cavity is given by a Boltzmann distribution in terms of the electrostatic potential $\Psi(r)$ at a distance r from its center,

$$\rho(r) = \bar{\rho} e^{q\Psi/k_B T}. \quad (22)$$

We choose $\Psi=0$ at the center of the cavity so that $\bar{\rho}$ is the actual charge density there. The charge density $-q\rho$ is also related to Ψ by Poisson’s equation,

$$\Delta\Psi = \frac{4\pi q\rho}{\epsilon}, \quad (23)$$

leading to the Poisson-Boltzmann equation³² which we conveniently express in the scaled form

$$\psi''(x) + \frac{2}{x} \psi'(x) = e^{\psi}. \quad (24)$$

Here, we have defined $\lambda^{-2} \equiv 4\pi Q\bar{\rho}$, $x \equiv r/\lambda$, and $\psi \equiv q\Psi/k_B T$, where λ may be interpreted as a screening length. The two additional boundary conditions are

$$\psi'(0) = 0 \quad (25)$$

owing to symmetry, and

$$\frac{b}{\lambda} \psi' \left(\frac{b}{\lambda} \right) = \Lambda \equiv \frac{QZ}{b} \quad (26)$$

signifying the relation between the electric field and the charge density at the surface of the cavity.

For small x , Eq. (24) admits a series expansion $\psi(x) = Ax^2 + Bx^4 + \dots$ with $A=1/6$ and $B=O(1)$ independent of the value of the dimensionless variable Λ . As Λ tends to zero, Eq. (26) reduces to the condition of electroneutrality. Electrostatic screening vanishes in this limit and there are no counterions “condensed” on the surface of the sphere. It is straightforward to solve Eq. (24) numerically starting with $\psi(x) \rightarrow \frac{1}{6}x^2$ as $x \rightarrow 0$. We have fitted the solution to the convenient approximation,

$$\psi(x) \approx -2 \ln \left(1 - \frac{x^2}{12} - \frac{x^4}{1440} - \frac{x^6}{45\,330.3} \right), \quad (27)$$

which is accurate to within 0.6% for $0 \leq x \leq 3.273\,687$ [$\psi(x)$ diverges at $x \approx 3.273\,687\,34$]. This leads to an effective charge given by

$$Z_{\text{eff}} \equiv \frac{4\pi b^3 \bar{\rho}}{3} = \frac{Z}{3\Lambda} \left(\frac{b}{\lambda} \right)^2. \quad (28)$$

This is always less than the actual charge Z which one may interpret as a certain fraction of counterions being associated near the surface if $\Lambda > 0$. The effective charge Z_{eff} tends to Z as $\Lambda \rightarrow 0$ (for a general analysis of this limit, see Appendix B).

We now wish to analyze the thermodynamic properties of the crystal in the presence of simple salt which we do within a Donnan approximation. At this stage it is well to recall the incorrectness of applying Donnan arguments to a fluid of charged colloidal particles. The probability of the double layers of two particles interpenetrating is very small owing to Boltzmann weighting. Hence, only the Debye-Hückel tails in their interaction are important which repre-

TABLE IV. The ionic strength I , the actual number of charges Z , the effective number Z_{eff} the chemical potential μ , and the osmotic pressure Π for a lysozyme crystal (the reference chemical potential has been set equal to zero).

pH	I (% w/v)	I (M)	Z	Λ	b/λ	Z_{eff}	w	$\frac{\mu}{k_B T}$	$\frac{\Pi v_0}{k_B T}$
4.0	2.0	0.40	11.1	5.51	2.52	4.27	1.41	2.83	1.92
4.0	3.0	0.57	11.2	5.56	2.53	4.29	2.00	2.07	1.43
4.0	4.0	0.74	11.4	5.66	2.54	4.32	2.57	1.64	1.14
4.0	5.0	0.92	11.6	5.76	2.55	4.35	3.14	1.36	0.95
4.0	7.0	1.26	11.7	5.81	2.55	4.37	4.30	1.01	0.71
4.5	2.0	0.40	10.2	5.06	2.48	4.13	1.45	2.66	1.81
4.5	3.0	0.57	10.3	5.11	2.49	4.15	2.06	1.94	1.34
4.5	4.0	0.74	10.3	5.11	2.49	4.15	2.68	1.52	1.06
4.5	5.0	0.92	10.4	5.16	2.49	4.17	3.28	1.25	0.88
4.5	7.0	1.26	10.4	5.16	2.49	4.17	4.51	0.92	0.64
5.4	2.0	0.40	9.1	4.52	2.42	3.94	1.53	2.42	1.66
5.4	3.0	0.57	9.1	4.52	2.42	3.94	2.18	1.75	1.21
5.4	4.0	0.74	9.2	4.57	2.43	3.95	2.81	1.38	0.96
5.4	5.0	0.92	9.2	4.57	2.43	3.95	3.46	1.13	0.79
5.4	7.0	1.26	9.1	4.52	2.42	3.94	4.77	0.82	0.58

sent effectively the potential of mean force between the particles. In the case of excess salt, we then use the McMillan-Mayer theory to calculate the statistical mechanical properties of the fluid as has been done in Sec. II [see Eq. (2); this line of argumentation goes back to Stigter³⁴]. The situation is decidedly different when the particles are positionally ordered as in a crystal. The double layers are forced to overlap in that case. A usual (Donnan) approximation is then to suppose those points at zero electric field are in equilibrium with the reservoir.³² For the cavities in the crystal, this yields

$$I_c(\bar{\rho} + I_c) = I^2 \quad (29)$$

in view of the equality of the chemical potentials of the small ions in the respective phases. The osmotic pressure is given by the additivity rule as argued by Oosawa for polyions within conventional cell models,³²

$$\Pi = (\bar{\rho} + 2I_c - 2I)k_B T = \bar{\rho}k_B T[\sqrt{1 + w^2} - w], \quad (30)$$

$$w \equiv \frac{2I}{\bar{\rho}}.$$

The ions have been considered as ideal and the electrostatic stress is zero in Eq. (20). The chemical potential of the charged cavity, accurate to the same level of approximation, is readily computed from Eq. (30) (this is analogous to similar calculations for cell models of long charged rods³⁵),

$$\mu = \mu_{\text{ref}} + \frac{Z_{\text{eff}}k_B T}{2} \ln \left[\frac{\sqrt{1 + w^2} + 1}{\sqrt{1 + w^2} - 1} \right], \quad (31)$$

where μ_{ref} is a reference chemical potential independent of the concentration of salt, and not identical with μ_0 of Sec. II. Because the number of particles in the crystal is equal to the number of cavities, Eq. (31) also represents the chemical potential of a charged sphere carrying Z charges but with a different μ_{ref} .

A. Comparison with experiment

1. Lysozyme crystal

The volume per lysozyme molecule in the tetragonal crystal is 29.6 nm^3 (see Sec. III B). The radius of the effective sphere is 1.60 nm so the volume of a cavity is 12.4 nm^3 and $b=1.43 \text{ nm}$. In Table IV, we show values of Z as a function of the ionic strength I at three values of the pH. From these we calculate the dimensionless quantities Λ , b/λ , and Z_{eff} via the Poisson-Boltzmann equation. Then the pressure and the chemical potential are evaluated using Eqs. (30) and (31) (see Table IV). The curves in Fig. 7 represent the chemical potential computed in this manner together with the predictions from the theory of the liquid state as displayed in Fig. 2. The former have been shifted by an amount which is unknown in the present theory.

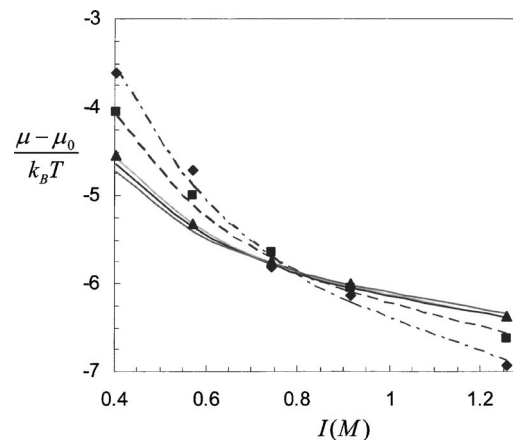


FIG. 7. The chemical potential of lysozyme in the fluid phase as a function of the ionic strength at pH 4.0 (diamonds), pH 4.5 (squares), and pH 5.4 (triangles) (see Fig. 2). The solid lines denote predictions from the theory of the crystalline state [Eq. (31)], with the effective charge from Table IV. The shift in chemical potential in units of $k_B T$ has been chosen to be 7.4 (light gray line, pH 4.0), 7.3 (black line, pH 4.5), and 7.15 (dark gray line, pH 5.4), respectively. The dashed line denotes the theory of the crystal for $Z_{\text{eff}}=5.0$ (shift=7.9) and the dash-dotted line for $Z_{\text{eff}}=5.9$ (shift=8.7).

TABLE V. Same as Table IV but now for $X_4\text{STA}\cdot n\text{H}_2\text{O}$. Here $n=31$ when $X=\text{H}$, $n=25$ when $X=\text{Li}$ and $n=18$ when $X=\text{Na}$.

X	I (% w/v)	I (M)	Z	Λ	b/λ	Z_{eff}	w	$\frac{\mu}{k_B T}$	$\frac{\Pi v_0}{k_B T}$
H	1.0	0.60	4.0	4.789	2.452	1.67	0.629	2.08	0.738
H	2.0	1.20	4.0	4.789	2.452	1.67	1.257	1.22	0.466
H	3.0	1.81	4.0	4.789	2.452	1.67	1.886	0.85	0.332
H	4.0	2.41	4.0	4.789	2.452	1.67	2.514	0.65	0.256
H	5.0	3.01	4.0	4.789	2.452	1.67	3.143	0.52	0.207
Li	1.0	0.60	4.0	5.134	2.488	1.61	0.531	2.23	0.950
Li	2.0	1.20	4.0	5.134	2.488	1.61	1.062	1.35	0.626
Li	3.0	1.81	4.0	5.134	2.488	1.61	1.594	0.95	0.455
Li	4.0	2.41	4.0	5.134	2.488	1.61	2.125	0.73	0.353
Li	5.0	3.01	4.0	5.134	2.488	1.61	2.656	0.59	0.288
Na	1.0	0.60	4.0	5.721	2.542	1.51	0.410	2.45	1.374
Na	2.0	1.20	4.0	5.721	2.542	1.51	0.819	1.55	0.970
Na	3.0	1.81	4.0	5.721	2.542	1.51	1.229	1.12	0.728
Na	4.0	2.41	4.0	5.721	2.542	1.51	1.639	0.87	0.575
Na	5.0	3.01	4.0	5.721	2.542	1.51	2.049	0.71	0.473

2. STA crystals

In order to compute the chemical potential we first need to discuss the crystal habits of STA. It is known that H_4STA is fully dissociated for a $p\text{H}$ larger than 5.³⁶ Zukoski and co-workers,^{5,30,37} failed to mention the $p\text{H}$ at which their measurements were performed, though they did deduce that all forms of STA are dissociated in their experiments judging from the conductivities of their solutions.

a. $\text{H}_4\text{STA}\cdot 31\text{H}_2\text{O}$. This crystallizes at room temperature³⁸ in the tetragonal form (long axis=1.856 nm, short axes=1.301 nm,³⁹ there are two STA molecules per unit cell of 3.142 nm³). We have earlier set the radius of an STA ion equal to 0.55 nm (see Sec. III C) so the volume of H_2O per STA molecule is 0.874 nm³ or $b=0.593$ nm. In Refs. 5 and 37 the water content of this crystal is given in terms of the molecular formula $\text{H}_4\text{STA}\cdot 31\text{H}_2\text{O}$.

b. $\text{Li}_4\text{STA}\cdot 24\text{H}_2\text{O}/\text{Li}_4\text{STA}\cdot 26\text{H}_2\text{O}$. Kraus described two forms of Li_4STA with 24 H_2O and 26 H_2O molecules attached, respectively.⁴⁰ Both crystals are rhombohedral [short axes in both cases=1.559 nm, long axis=3.898 nm in the former, long axis=4.118 nm in the latter; the angle between the short axes=120° (Ref. 39)]. Kraus also mentioned that one Li ion should probably be replaced by one H ion. There are actually three different numbers quoted for the water content of $\text{Li}_4\text{STA}\cdot n\text{H}_2\text{O}$ in Refs. 5, 30, and 37: $n=21, 24$, and 26 ! We have opted for $n=25$, namely, the average number for the crystal habits generally accepted. As there are six STA molecules per unit cell, the volume of crystal per STA molecule is 1.406 nm³ and the radius of our effective cavity is $b=0.553$ nm.

c. $\text{Na}_4\text{STA}\cdot 18\text{H}_2\text{O}$. This crystallizes in the triclinic form within a narrow range around 308 K.³⁸ The absolute dimensions of the unit cell do not seem to be known. We thus estimate the amount of H_2O per STA molecule via the molecular formulas. The water content in $\text{Na}_4\text{STA}\cdot n\text{H}_2\text{O}$ is stated to be $n=18$ in Ref. 37 and $n=14$ in Ref. 5. The latter value seems too low and is possibly a misprint since n should be equal to 20 according to the usual citation.⁴¹ Accordingly, we adopt $n=18$ here to be used in the solubility studies.³⁰ A

molecule of H_2O has a volume of 0.0285 nm³ which is based on the amount of H_2O in the unit cells of $\text{H}_4\text{STA}\cdot 31\text{H}_2\text{O}$ and $\text{Li}_4\text{STA}\cdot 26\text{H}_2\text{O}$. Therefore, $\text{Na}_4\text{STA}\cdot 18\text{H}_2\text{O}$ has 0.513 nm³ H_2O per STA molecule so we have $b=0.496$ nm.

Overall, it is not clear how much H_2O is exactly present in the STA crystals. Fortunately, the chemical potential [Eq. (31)] depends only logarithmically on this quantity so the data compiled in Table V are not so sensitive to this type of uncertainty. The predicted chemical potentials are depicted as curves in Fig. 8 together with the computations from our theory of the liquid state (Fig. 5).

V. DISCUSSION

Except for a slight downward adjustment of the effective charge of lysozyme in the fluid phase, there are essentially no adjustable parameters in our analysis. The adjustment is

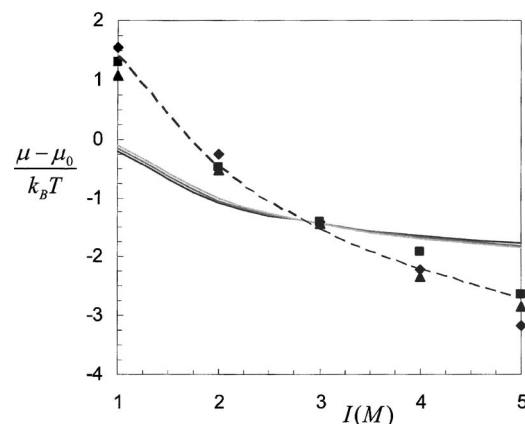


FIG. 8. Chemical potential of STA in the fluid phase as a function of the ionic strength (see Fig. 5). Salt added: LiCl (diamonds), HCl (squares), and NaCl (triangles) (counterion of STA is the same as that of the salt). The solid lines denote predictions from the theory of the crystalline state [Eq. (31)], with the effective charge from Table V. The shift in chemical potential in units of $k_B T$ is 2.3 (black line, $\text{H}_4\text{STA}\cdot 31\text{H}_2\text{O}$) 2.4 (dark gray line, $\text{Li}_4\text{STA}\cdot 25\text{H}_2\text{O}$), and 2.55 (light gray line, $\text{Na}_4\text{STA}\cdot 18\text{H}_2\text{O}$), respectively. The dashed line denotes predictions from the theory of the crystal for $Z_{\text{eff}}=2.8$ (shift=5.5).

by one unit only which is insignificant compared with the approximations inherent in the standard electrostatic theory. The adhesion parameters are completely constrained by the second virial curves (Figs. 1 and 4). We predict that the chemical potentials in the fluid and solid phases should coincide apart from an unimportant shift in the vertical offset because the reference potential is not known exactly for the crystal. This appears to be almost the case for lysozyme (see Fig. 7) but there is an appreciable disparity between the respective curves in the case of the silicotungstates (see Fig. 8). Nevertheless, we note that the shapes of the curves are the same which implies that the logarithmic form in Eq. (31) appears to be confirmed, i.e., the Donnan effect seems to apply to crystals of charged nanoparticles. This is borne out by adjusting Z_{eff} upward somewhat for both types of crystals. We then actually attain coincident curves (see Figs. 7 and 8). A further implication is that the precise crystal structure is unimportant with regard to the ionic-strength dependence of μ . Equation (31) results from approximating the cavities within the crystals by spheres; the detailed electrostatics is independent of the salt concentration.

The coexistence equation for the osmotic pressure yields little information [see Eq. (20)] because it is unclear at present how to relate the adhesive forces between spheres to the elastic properties of the crystal. To compute the latter we need insight in the forces between the particles at the angstrom level which we do not have at present. Adhesive interactions appear to play a minor role in the STA crystals for the fluid and crystal pressures are quite close (compare Table III and V). By contrast, in lysozyme crystals the osmotic pressure due to electrostatic forces is largely balanced by sticky interactions between touching protein molecules. In a similar vein there is a marked difference between the two colloids with regard to their respective ionic strengths under theta conditions when B_2 equals zero (see Figs. 1 and 4). These salt concentrations may be estimated with the help of Eq. (5). Although $\delta \exp U_A = 1.36$ for STA is not substantially less than the respective value 3.33 for lysozyme, the concentrations differ appreciably because of the exponential screening term multiplying the attraction in Eq. (5).

It is wise to emphasize the shortcomings in the approximations introduced in the electrostatic interactions. Discrete charge effects have been disregarded entirely. At the same level of approximation we have not addressed the electrostatics of the minutely thin boundary layers between almost touching spheres within the crystal phase. There are cavities at nanometer scales and these are assumed to give rise to the ionic-strength dependence of the free energy of the crystal. The Donnan approximation used suffers from the same drawback as always: the effective charge Z_{eff} is posited to be independent of the electrolyte in the crystal and thus the reservoir (the fluid phase in our case). It would be interesting to study the fluid-crystal coexistence of globular particles of low charge density. The counterions in the crystal would then be essentially free (see Appendix B) and there would be less uncertainty about the magnitude of the electrostatic interactions.

There is another potential problem in the fluid phases of silicotungstates. At 1M electrolyte, the solubilities of STA

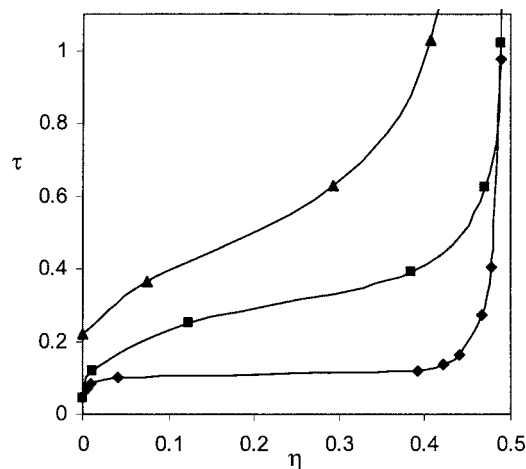


FIG. 9. Fluid branches of the fluid-crystal coexistence computed by simulation for the Yukawa interaction for several values of the inverse range of the interaction $\kappa\sigma=7$ (diamonds), $\kappa\sigma=25$ (squares), and $\kappa\sigma=100$ (triangles). The data were calculated using the theory from Refs. 7 and 8 and the simulations from Ref. 42. The lines are a guide to the eyes.

are remarkably high (see Table III). It would appear that the counterions arising from STA should contribute to the screening on a par with the salt ions. This is not borne out by the present analysis, however, since there is no leveling off of the chemical potentials in the crystal phases in Figs. 7 and 8. Nevertheless, a liquid state theory of concentrated charged nanoparticles needs to be developed in which the counterions are duly accounted for. We note that the interaction between the particles is not pairwise additive in that case.

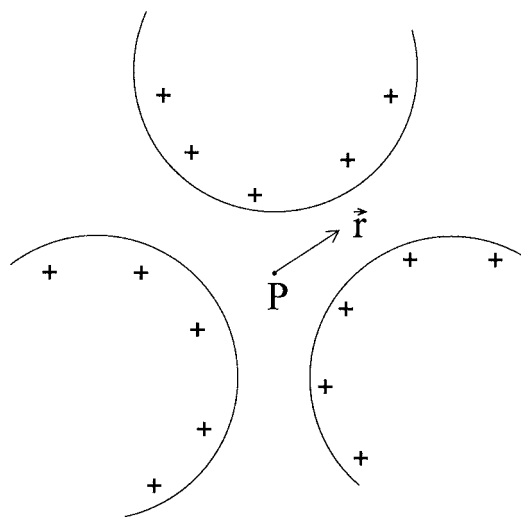
In summary, we have provided a semiquantitative explanation for the ionic-strength dependence of the fluid-crystal coexistence of suspensions of charged nanoparticles. We believe this explanation is especially forceful because we have considered two rather disparate types of globular particles in detail. In particular, the solubility curves of lysozyme and silicotungstate differ markedly, yet the curves for the chemical potentials turn out to have the same form.

ACKNOWLEDGMENT

The authors thank Professor E. Trizac for correspondence on the Poisson-Boltzmann equation.

APPENDIX A: PHASE DIAGRAM OF HARD SPHERES INTERACTING BY ATTRACTIVE YUKAWA FORCES

Dijkstra⁴² performed computer simulations, more elaborate than those carried out by Hagen and Frenkel,⁴³ on a system of hard spheres of diameter σ attracting each other by exponentially decaying forces (the Yukawa interaction). She varied both the amplitude β and the inverse range κ of the potential. The variable τ in the optimized Baxter model⁷ has been computed by us for the attractive Yukawa system.⁸ At fluid-crystal coexistence in Dijkstra's simulations, we evaluate τ from κ , β , and the volume fraction η of the fluid phase which is displayed as a function of η in Fig. 9. It is immediately seen that $\tau(\eta)$ is not a single universal curve but depends markedly on the range of the interaction also. Of course, this is not surprising: although τ is a correct similar-

FIG. 10. Point P in a void of the crystal.

ity variable for the fluid phase,⁸ it has nothing to do with the statistical properties of the crystal in which the configurations are weighted totally differently than those in the fluid.

APPENDIX B: POISSON-BOLTZMANN EQUATION IN A CRYSTAL OR POROUS MEDIUM

Here, we present only a sketch of a general analysis of the Poisson-Boltzmann equation for the electrostatic potential $\Psi(\mathbf{r})$ at position \mathbf{r} within the aqueous interstitial space inside a crystal (which may be considered to be a porous medium), under appropriate conditions. The particles in the crystal are positively charged and simple salt is absent at first. The potential is again related to the counterion density $\rho(\mathbf{r})$ via the Poisson equation (23). Now it is possible to discern some point P in the void between several particles where the potential is a local minimum and where the density is $\bar{\rho}_P(0)$ (see Fig. 10). Point P is chosen as the origin.

If the potential is scaled analogously as in Sec. IV, we have $\rho(\mathbf{r}) = \bar{\rho}_P \exp \psi(\mathbf{r})$ [see Eq. (22)]. Thus, the Poisson-Boltzmann equation may be written as

$$\Delta \psi = \lambda_P^{-2} e^\psi, \quad (\text{B1})$$

where the screening length λ_P is given by $\lambda_P^{-2} = 4\pi Q \bar{\rho}_P$.

In general, it is difficult to address (B1) because λ_P is unknown. But it is possible to progress if we suppose $|\mathbf{d}| \leq \lambda_P$ where $|\mathbf{d}|$ is the largest vector distance between P and a point on the surface of the surrounding spheres (i.e., those belonging to a cluster enclosing the void centered on P). An inner solution of (B1) must have the form $\psi_{\text{in}}(\mathbf{r}/\lambda_P)$ and may be written as a Taylor expansion to second order,

$$\psi_{\text{in}}(\mathbf{r}) = \frac{1}{2} \mathbf{r} \mathbf{r} : \left. \frac{\partial^2 \psi_{\text{in}}}{\partial \mathbf{r} \partial \mathbf{r}} \right|_{\mathbf{r}=0}, \quad (\text{B2})$$

if $|\mathbf{d}| \leq \lambda_P$. There is an outer solution ψ_{out} needed to accommodate for the complicated boundaries. Then, we have a boundary condition on the electric field at $\mathbf{r} = \mathbf{d}$ in terms of ψ_{out} which we rewrite in terms of ψ_{in}

$$\mathbf{n} \cdot \left. \frac{\partial \psi_{\text{in}}}{\partial \mathbf{r}} \right|_{\mathbf{r}=\mathbf{d}} = \mathbf{n} \mathbf{d} : \left. \frac{\partial^2 \psi_{\text{in}}}{\partial \mathbf{r} \partial \mathbf{r}} \right|_{\mathbf{r}=0} = 4\pi k_1 \sigma_b Q. \quad (\text{B3})$$

Here, σ_b is the uniform density of charge on a sphere and k_1 is a numerical coefficient of order unity associated with the matching of the inner and outer solutions. The effect of an internal permittivity is disregarded. The left-hand side of (B3) scales as λ_P^{-2} implying that $\bar{\rho}_P$ must be proportional to σ_b . In view of electroneutrality we also require the average of $\rho(\mathbf{r})$ to be proportional to σ_b . Hence, the potential $\psi(\mathbf{r})$ must be very small, which is consistent with the initial Ansatz (B2). We conclude that for small enough cavitylike voids, the density of counterions is approximately constant so that the effective charge density is virtually equal to the actual charge density. In that case, when the crystal is immersed in a reservoir containing monovalent electrolyte, Eqs. (30) and (31) are valid with $\bar{\rho}$ simply given by the concentration of counterions in the interstitial space between the spheres; $Z_{\text{eff}} = Z$ in Eq. (31). Because $|\mathbf{d}| = O(a)$, we ultimately require $ZQ/a \ll 1$ as a necessary and sufficient condition for this to hold true. In the spherical cavity approximation introduced in Sec. IV, we have $b = O(a)$ so $\Lambda \ll 1$ is effectively the same requirement (which led to $Z_{\text{eff}} = Z$).

- ¹A. George and W. W. Wilson, *Acta Crystallogr., Sect. D: Biol. Crystallogr.* **D50**, 361 (1994).
- ²A. George, Y. Chiang, B. Guo, A. Arabshahi, Z. Cai, and W.W. Wilson, *Methods Enzymol.* **276**, 100 (1997).
- ³B. Guo, S. Kao, H. McDonald, A. Asanov, L.L. Combs, and W.W. Wilson, *J. Cryst. Growth* **196**, 424 (1999).
- ⁴C. Haas, J. Drenth, and W.W. Wilson, *J. Phys. Chem. B* **103**, 2808 (1999).
- ⁵D. Rosenbaum, P.C. Zamora, and C.F. Zukoski, *Phys. Rev. Lett.* **76**, 150 (1996).
- ⁶D. F. Rosenbaum and C.F. Zukoski, *J. Cryst. Growth* **169**, 752 (1996).
- ⁷P. Prinsen and T. Odijk, *J. Chem. Phys.* **121**, 6525 (2004).
- ⁸P. Prinsen, J.C. Pàmies, T. Odijk, and D. Frenkel, *J. Chem. Phys.* (to be published), e-print cond-mat/0603716.
- ⁹C. Haas and J. Drenth, *J. Phys. Chem. B* **102**, 4226 (1998).
- ¹⁰C. Haas and J. Drenth, *J. Cryst. Growth* **196**, 388 (1999).
- ¹¹R. A. Curtis, H.W. Blanch, and J.M. Prausnitz, *J. Phys. Chem. B* **105**, 2445 (2001).
- ¹²E. Cacioppo and M.L. Pusey, *J. Cryst. Growth* **114**, 286 (1991).
- ¹³M. Boström, D.R. M. Williams, and B.W. Ninham, *Langmuir* **17**, 4475 (2001).
- ¹⁴F. W. Tavares, D. Bratko, H.W. Blanch, and J.M. Prausnitz, *J. Phys. Chem. B* **108**, 9228 (2004).
- ¹⁵M. Aubouy, E. Trizac, and L. Bocquet, *J. Phys. A* **36**, 5835 (2003).
- ¹⁶R. Fowler and E.A. Guggenheim, *Statistical Thermodynamics* (Cambridge University Press, Cambridge, 1956).
- ¹⁷W. C. K. Poon, S.U. Egelhaaf, P.A. Beales, A. Salonen, and L. Sawyer, *J. Phys.: Condens. Matter* **12**, L569 (2000); P.B. Warren, *ibid.* **14**, 7617 (2002).
- ¹⁸R. J. Baxter, *J. Chem. Phys.* **49**, 2770 (1968).
- ¹⁹H. C. Andersen, J.D. Weeks, and D. Chandler, *Phys. Rev. A* **4**, 1597 (1971).
- ²⁰J. P. Hansen and I.R. McDonald, *Theory of Simple Liquids* (Academic, London, 1976).
- ²¹B. Barbo, *J. Chem. Phys.* **61**, 3194 (1974).
- ²²L. K. Steinrauf, *Acta Crystallogr.* **12**, 77 (1959).
- ²³A. Nadarajah and M.L. Pusey, *Acta Crystallogr., Sect. D: Biol. Crystallogr.* **52**, 983 (1996).
- ²⁴V. Mikol, E. Hirsch, and R. Giegé, *J. Mol. Biol.* **213**, 187 (1990).
- ²⁵D. E. Kuehner, J. Engmann, F. Fergg, M. Wernick, H. W. Blanch, and J. M. Prausnitz, *J. Phys. Chem. B* **103**, 1368 (1999).
- ²⁶M. Riès-Kautt, A. Ducruix, and A. van Dorselaer, *Acta Crystallogr., Sect. D: Biol. Crystallogr.* **50**, 366 (1994).
- ²⁷M. Ge, A. A. Gewirth, W. G. Klempere, and C. G. Wall, *Pure Appl.*

- Chem. **69**, 2175 (1997).
- ²⁸M. C. Baker, P. A. Lyons, and S. J. Singer, *J. Am. Chem. Soc.* **77**, 2011 (1955).
- ²⁹T. Kurucsev, A. M. Sargeson, and B. O. West, *J. Phys. Chem.* **61**, 1567 (1957).
- ³⁰C. F. Zukoski, D. F. Rosenbaum, and P. C. Zamora, *Chem. Eng. Res. Des.* **74**, 723 (1996).
- ³¹L. D. Landau and E. M. Lifshitz, *Theory of Elasticity*, 3rd ed. (Pergamon, Oxford, 1986).
- ³²F. Oosawa, *Polyelectrolytes* (Dekker, New York, 1971).
- ³³T. Odijk, *Philos. Trans. R. Soc. London, Ser. A* **362**, 1497 (2004).
- ³⁴D. Stigter, *Biopolymers* **16**, 1435 (1977).
- ³⁵T. Odijk and F. Slok, *J. Phys. Chem. B* **107**, 8074 (2003).
- ³⁶M. J. Kronman and S. N. Timasheff, *J. Phys. Chem.* **63**, 629 (1959).
- ³⁷P. C. Zamora and C. F. Zukoski, *Langmuir* **12**, 3541 (1996).
- ³⁸G. Wyrouboff, *Z. Kristallogr.* **29**, 659 (1898).
- ³⁹H. T. Evans, in *Perspectives in Structural Chemistry*, edited by J. D. Dunitz and J. A. Ibers (Wiley, New York, 1971), Vol. IV, pp. 8–21.
- ⁴⁰O. Kraus, *Z. Kristallogr.* **94**, 256 (1936).
- ⁴¹R. J. Meyer, *Gmelins Handbuch der Anorganischen Chemie, Wolfram*, (Verlag Chemie, Berlin, 1933).
- ⁴²M. Dijkstra, *Phys. Rev. E* **66**, 021402 (2002).
- ⁴³M. H. J. Hagen and D. Frenkel, *J. Chem. Phys.* **101**, 4093 (1994).